Journal of Electrotechnology, Electrical Engineering and Management (2024)
Clausius Scientific Press, Canada
DOI: 10.23977/jeeem.2024.070116
ISSN 2560-6697 Vol. 7 Num. 1

Design and performance analysis of intelligent variable flux built-in permanent magnet synchronous motor

Hui Zhang*, Hongfei Yin, Fangning Li, Ruiping Jiang

College of Computer and Control Engineering, Qiqihar University, Qiqihar, Heilongjiang, 161000, China

Corresponding author: zh@qqhru.edu.cn

Keywords: Mechanical device with variable flux, permanent magnet synchronous machine, rotating magnetic pole, electromagnetic characteristic, finite element analysis

Abstract: In view of the existing variable flux permanent magnet synchronous motor with limited range of magnetization and no automatic control of magnetization accuracy, an intelligent variable flux permanent magnet synchronous motor with auto-rotating permanent magnets and rotor built-in drive controller (IVFPMSM) is proposed. This paper analyzes the internal structure design and operation principle of this intelligent variable flux permanent magnet synchronous motor (IVFPMSM), and numerically analyzes the electromagnetic characteristics such as induced electric potential, winding magnetic chain, air gap flux density and weak magnetic characteristics when the permanent magnets (PMs) rotate at 0 °, 30 °, 45 °and 90 °, respectively. The results show that the PM can be rotated at any angle under the composite drive, which greatly widens the range of motor magnetization. The validity of the theory and design is verified by making a prototype and building a test platform.

1. Introduction

Permanent magnet motors have better performance than other motors under the same operating conditions and are widely used in various fields [1-4]. However, the conventional permanent magnet motor has problems such as the difficulty of permanent magnet field adjustment, which has been limiting the development of permanent magnet motor. To address these problems, researchers have proposed a variable flux motor (VFM) with adjustable air-gap magnetic field strength. The concept of adjustable flux motor has attracted a lot of attention in the industry, so different principles and different structures of this type of motor have been proposed one after another. At the same time, the problems in the magnetic field regulation process have been studied and various motor magnetic regulation control strategies have been proposed.

Various topology motors have been proposed by domestic and foreign scholars[5-6], and the University of Wisconsin-Madison proposed an adjustable flux motor with AC axis reluctance enhancement and an axial flux adjustable motor [7-8]. References [9-11] proposed a series of adjustable parallel flux machines, and references [12-13] introduced the concept of memory motors to stator permanent magnet motors and proposed a biconvex adjustable flux motor. References [14-15] proposed a variety of series-parallel hybrid adjustable flux motors. Reference [16] proposed an adjustable flux motor with a semi-series structure. Reference [17-18] proposed a mechanically

adjustable flux motor. References [19-20] proposed a pole rotating variable flux permanent magnet synchronous motor. All of the above motors can be controlled by magnetic chains. However, the range of magnetic field adjustment is limited, the accuracy of magnetic adjustment cannot be automatically controlled, and the adaptability to different working conditions is poor, etc.

To address the above problems, this paper proposes an intelligent permanent magnet synchronous motor with auto-rotating PMs, a rotor with built-in driver, and a rotor sensing function. The electromagnetic simulation model of the motor is established, its motor structural characteristics and operating principle are analyzed, the rotor sensing control circuit is designed and built, and the electromagnetic characteristics of the motor, such as the induced electric potential, winding magnetic chain and air gap flux density, are numerically analyzed under different angles of the magnetic pole by establishing the simulation model; meanwhile, a prototype is made for experimental study to verify the validity of the theoretical design and simulation.

2. Modeling

2.1. The Structure of the IVFPMSM

The IVFPMSM has a variable structure rotor with four rotating PMs mounted symmetrically inside the rotor, and the four PMs are connected to four servo motors. At the end of the rotor shaft of the motor, a controller and a power generation source are installed to supply and control the relevant equipment to realize the closed-loop position control of the rotating magnetic poles. Such a design scheme makes the motor have the advantages of automatic adjustment of magnetic pole direction, wide range of magnetic field adjustment, high accuracy of adjustment and strong adaptability. It changes the traditional motor structure and provides a new idea and direction for the optimization of motor performance and intelligent development.

The overall motor assembly is shown in Figure 1. The motor body includes end caps, permanent magnets, stator, rotor, windings, spindle and bearings. The motor rotor is embedded with a magnetic drive control device consisting of gears and a DC servo motor, and the spindle end is equipped with a self-generating device, sensors and other detection devices.

The part of the rotating shaft is shown in Figure 2. In order to facilitate the connection and current transmission between the self-electric device and the internal drive device, the hollow rotating shaft design will be adopted, and the positions close to the two ends of the shaft will be perforated to facilitate the installation of the control circuit board. Considering the pressure and friction of the bearing at work, the hardness and wear resistance of the material, and the high elastic limit, the 45 steel with good mechanical properties is selected.

The magnetic regulating device and the rotating shaft are assembled by bearings, and are composed of gears, flanges and DC servo motors. The flange plate is arranged with four small gears connected with the DC servo motor and four big gears connected with the rotating magnetic pole; The magnetic regulating device runs synchronously with the rotor, the DC servo motor is powered on, and the rotation of the pinion drives the rotation of the big gear to realize the rotation of the magnetic pole. The schematic diagram of the magnetic regulating device is shown in Figure 3.

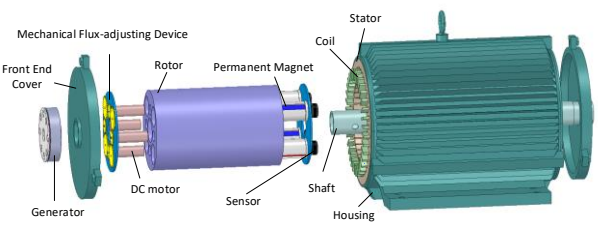

Figure 1: IVFPMSM

Figure 2: Shaft

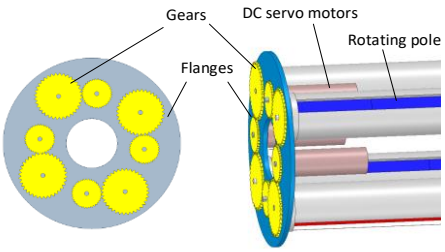

Figure 3: Magnetizing devices

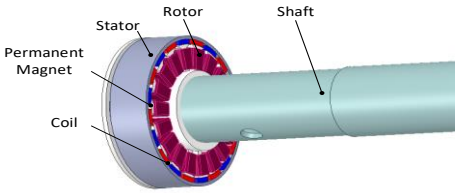

Figure 4: Self-generating devices

Four rotatable poles are installed on the rotor of the motor, and a magnetizing drive device consisting of gears and DC servo motors is connected to each PMs. The magnetizing drive control device controls the rotation of each PMs at any angle, and an angle sensor is installed at the PMs to detect the PMs position in real time. At the same time, a small self-generating device is installed at the end of the motor shaft. Its structure is shown in the figure 4. The self-generating device adopts a permanent magnet generator, whose rotor moves with the main shaft, and the generator shell is fixed with an aluminum sheet. The main shaft rotates to drive the generator rotor to rotate and generate electricity, so as to supply power to the magnetic regulating drive control device, sensor and other detection devices on the rotor of the variable structure motor.

2.2. The Principle of the IVFPMSM

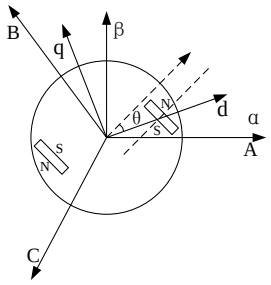

Figure 5: Coordinate system

The coordinate system of IVFPMSM is shown in Figure 5, because the angle of its rotor permanent magnet can be changed, so assume that the angle between the direction pointed by the N pole of the

permanent magnet and the direction of the initial position is θ, and the rotor flux is φ_f, then the component of the rotor flux in the d-axis after the rotation of the permanent magnet is $\varphi_f \cos\theta$, and the component in the q-axis is $\varphi_f \sin\theta$. Based on the above assumptions, the direct cross-axis magnetic chain relationship can be obtained by transformation as

$$\begin{cases} \varphi_d = \varphi_f \cos\theta + L_d i_d \\ \varphi_q = \varphi_f \sin\theta + L_q i_q \end{cases}$$

Where, φ_f is the rotor flux; θ is the angle between the rotor pole and the d-axis; L_d and L_q are the inductance of the dq-axis.

the voltage equation in the dq-axis coordinate system is:

$$\begin{cases} u_d = R_s i_d - \omega_e \varphi_q + \dfrac{d\varphi_d}{dt} \\ u_q = R_s i_q + \omega_e \varphi_d + \dfrac{d\varphi_q}{dt} \end{cases}$$

Where, u_d and u_q are the voltage of dq axis; R_s is the stator resistance; i_d and i_q are the current of dq axis; ω_e is the electromagnetic speed; φ_d and φ_q are the magnetic flux of dq axis.

Flux linkage equation:

$$\begin{cases} \psi_d = L_d i_d + L_{md} \psi_f{}' * \cos\alpha / L_{md} \\ \psi_q = L_q i_q \end{cases}$$

Where, L_d and L_q are the inductors of the dq axis of the stator winding, L_{md} is the D-axis mutual inductance between fixed and rotor; i_f is the equivalent excitation current of a permanent magnet, $i_f = \psi_f / L_{md}$; $\psi_f = \psi_f{}' * \cos\alpha$, $\psi_f{}'$ is the rotation Angle.

It can be seen that reducing the permanent magnet chain and adjusting the direct cross-axis current component can make the motor achieve the purpose of weak magnetic speed regulation.

Torque equation:

$$T_{em} = p\left(\psi_d i_q - \psi_q i_d\right) = p\left[L_{md} i_f i_q + \left(L_d - L_q\right) i_d i_q\right]$$

Where, T_{em} is electromagnetic torque; p is the number of poles of the motor.

If the relevant quantity in the above formula is expressed as a space vector, then

$$u_s = u_d + j u_q = R_1 i_s + \frac{d\psi_s}{dt} + j\omega\psi_s$$

$$i_s = i_d + j i_q$$

$$\psi_s = \psi_d + j\psi_q$$

$$T_{em} = p\psi_s \times i_s = p\,\mathrm{Re}\left(j\psi_s i_s^*\right)$$

Where, i_s^* is the complex conjugate of i_s. The corresponding space vector diagram is shown in Figure 6.

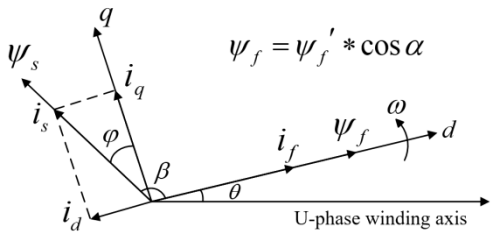

Figure 6: Vector image

3. Rotor Built-in Drive Control Circuit Design

The internal control circuit of IVFPMSM consists of five parts: power supply part, STM32 system part, DC motor driver part, encoder interface part and ESP8266 part.

As shown in Figure 7, in the power supply section, the alternating current output from the generator is connected to the control circuit through the P1 socket and changed to direct current through the D1 rectifier bridge and C1 capacitor filter. The rectified power supply passes through U1(LM2596), U3(SCT2360) and U7(AMS1117S) voltage regulator chips, which are stepped down to 12V, 5V and 3.3V, respectively, to accommodate the voltage requirements of different chips.

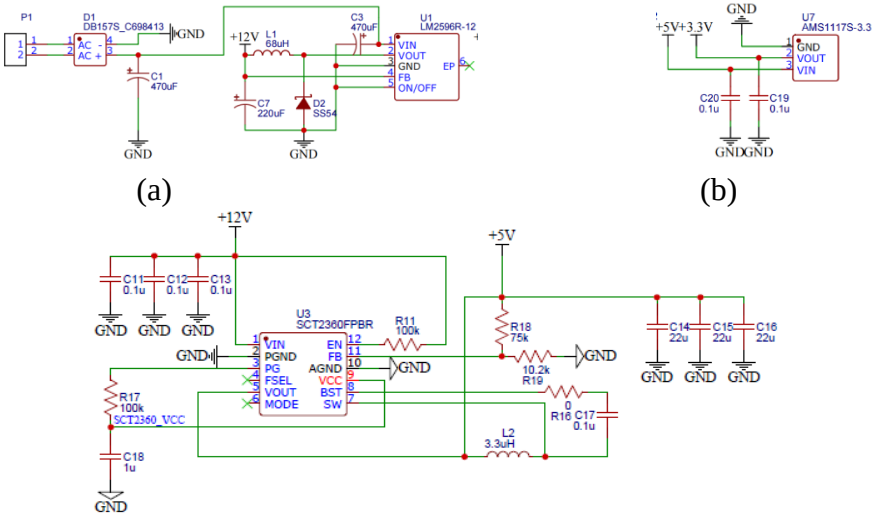

Figure 7: Rotor power conversion circuit

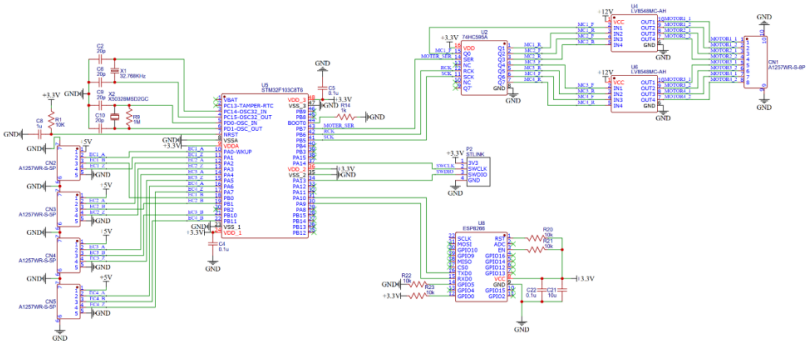

Figure 8: Rotor built-in drive control system

As shown in Figure 8, the STM32 system part consists of STM32 microcontroller, reset circuit, crystal circuit, BOOT selection circuit and STLINK interface. The motor drive circuit consists of U2(74HC595A) and U4 and U6(LV8548MC). Among them, 74HC595A is a serial input and parallel output displacement buffer. LV8548MC is a motor driver chip, each LV8548MC chip can drive two motors, IN1 and IN2 are the control signal input pins of the first circuit, OUT1 and OUT2 are the output pins of the first circuit. IN3 and IN4 are the control signal input pins of the second circuit. OUT1 and OUT2 are the output pins of the second circuit. The STM32 outputs 8-bit serial encoded data to the 74HC595A, which is converted and output in parallel by the Q0～Q7 pins of the 74HC595A. Q0～Q3 are output to IN1～IN4 of U4 to control motor 1 and motor 2. Q4～Q7 are output to IN1～IN4 of U6 to control motor 3 and motor 4. The encoder interface CN2～CN5 is used to connect the encoder. Four 360-line optical encoders are used in this design to measure the rotation angle of the variable pole. Each encoder can output three phase square wave signals, A, B and Z. The phase difference between A and B is 90 °, and the direction of pole rotation can be determined by the overrun or lag of phase A relative to phase B. The pole rotation angle can be obtained by counting the pulses, and the zero pulse of phase Z can be used to correct the counting error. Through WiFi connection, the controller can send the collected motor status to the host computer, and also receive action commands from the host computer.

4. Electromagnetic Performance Analysis

4.1. Partial Parameters of IVFPMSM

The partial parameters of IVFPMSM are set as shown in Table 1.

Table 1: Partial parameters of IVFPMSM.

Item	Value	Item	Value
Number of phases	3	Rated power/kw	7.5
Stator outer diameter/mm	210	Rated speed/rpm	1400
Stator axial length/mm	255	Rated current/A	15
Rotor outer diameter/mm	134	Air gap length/mm	0.5
Rotor inner diameter/mm	42	Number of PMs	4
Rotor axial length/mm	215	winding connection	Wye

4.2. The Distribution of Magnetic Field

Using the finite element method, the two-position Maxwell electromagnetic field equation of the motor is analyzed:

$$\Omega: \frac{\partial}{\partial x}\left(v\frac{\partial y}{\partial x}\right)+\frac{\partial}{\partial y}\left(v\frac{\partial y}{\partial x}\right)=-J-v\left(\frac{\partial B_{zy}}{\partial x}-\frac{\partial B_{zx}}{\partial y}\right)+\sigma\frac{\partial A}{\partial t}$$

Where, Ω Where, represents the calculation field solution region, A represents the magnetic field vector, J represents the current density, v represents the magnetic resistance, σ represents the electrical conductivity, B_{zx} and B_{zy} represents the remanent magnetic density in x direction and y direction respectively.

The above formula is discretized by finite element method, and the formula can be obtained by weighted average:

$$\iint\left(\{N\}^T\left[\frac{\partial}{\partial x}\left(\frac{1}{\mu}\frac{\partial A}{\partial x}\right)+\frac{\partial}{\partial y}\left(\frac{1}{\mu}\frac{\partial A}{\partial y}\right)\right]+\{N\}^T J_z-\{N\}^T\sigma\frac{dA}{dt}\right)dxdy=0$$

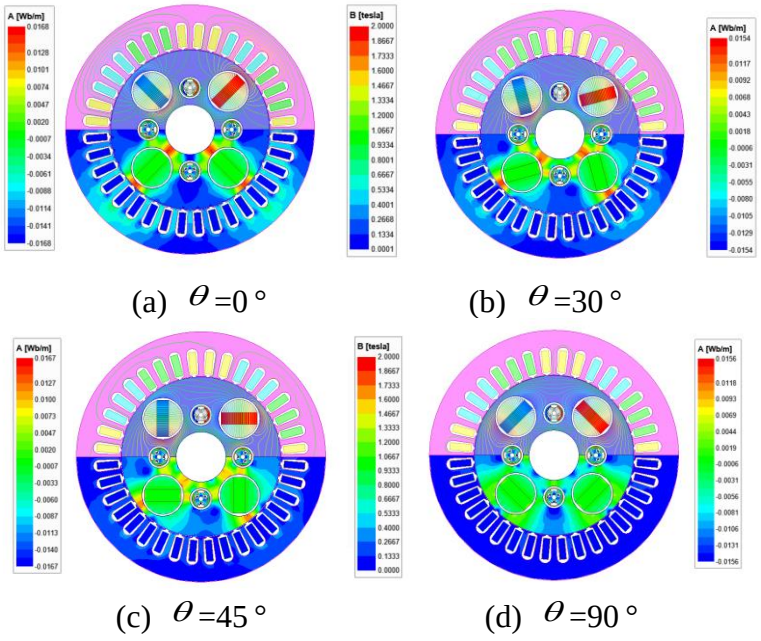

(a) θ=0° (b) θ=30°

(c) θ=45° (d) θ=90°

Figure 9: The Distribution of Magnetic Field

Figure 9 shows the distribution of magnetic lines of force and magnetic density clouds inside the motor under different rotation angles. The motor is driven with four poles rotating synchronously at an angle θ, where the motor is equivalent to a conventional permanent magnet synchronous motor at θ=0°, and the excitation magnetic field is generated by the permanent magnet, at which time the internal magnetic field of the motor is the largest, and the magnetic field distribution is shown in Fig. 9(a); compared with θ=0°, the magnetic lines of the stator turn chain decrease sharply at θ=45°, and most of the magnetic lines are distributed in the rotor, and the rotor core near the d-axis becomes saturated, and the main flux through the main magnetic flux through the air gap into the stator is greatly reduced. When θ=90°, as shown in Figure 9(d), the permanent magnets only interact with their adjacent magnets of opposite polarity, so that the main flux into the stator core is extremely small, thus realizing a wide range of weak magnetization of the motor.

Therefore, by rotating the permanent magnet at a large Angle, the magnetization direction of the permanent magnet can be changed, and the internal air gap magnetic field can be properly adjusted to play a good weak magnetic property.

4.3. Winding Flux Linkage and EMF

The electromotive force can be expressed as

$$E_0 = 4.44 f N K_{dp1} \Phi_m$$

Where, f is the rated frequency of the motor; N is the number of turns in series of each phase of armature winding; K_{dp1} is winding coefficient; Φ_m is no-load air gap flux.

Figure 10 shows EMF of phase A at different rotation angles of PMs.Figure 11 shows odd harmonic analysis of no-load induced EMF. As the rotation Angle of PMs increases, the no-load induced EMF of motor decreases linearly. The maximum induced EMF is 61V when θ=0°. When

θ =90 °, the induced EMF is the smallest and the fluctuation is gentle, and the maximum value is 3V. The simulation results show that magnetic weakening can be achieved by controlling the rotation of PMs.

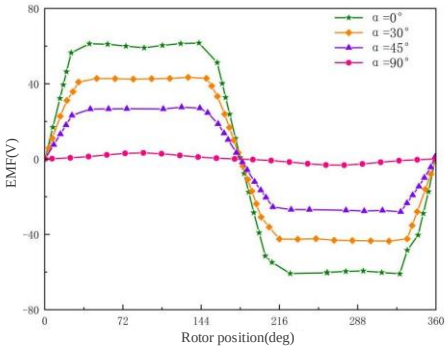

Figure 10: The induced EMF of IVFPMSM

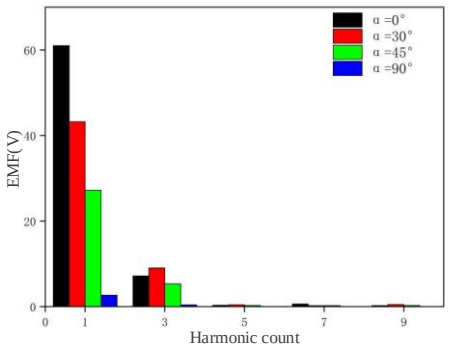

Figure 11: Harmonics

The distribution of winding flux linkages for the motor at different PMs rotation angles is shown in Figure 12. As the PMs rotation angle gradually increases, the magnitude of the magnetic chain decreases. This is due to the fact that the magnetization direction of a single PM changes with respect to its initial position after it is rotated by a certain angle, resulting in a decrease in the component of the winding magnetic chain in the d-axis direction.

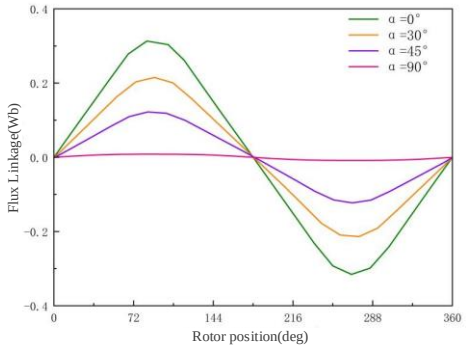

Figure 12: The flux linkage of IVFPMSM

The weak magnetic ratio and flux amplitude at different rotation angles of PMs under no-load condition are shown in Figure 13. It can be seen that the amplitude of the winding flux decreases with the increase of the magnetic pole rotation Angle, and the weak magnetic ratio increases gradually. Under the condition of unsaturated motor, the weak magnetic ratio can be as high as 97.5% at no load, which has a very good weak magnetic effect.

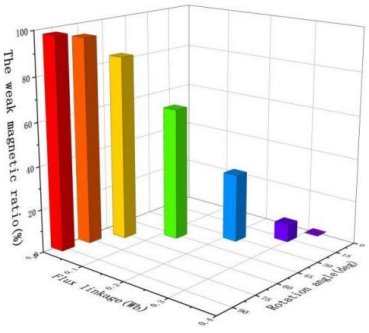

Figure 13: The weak magnetic ratio

4.4. Air Gap Flux Density

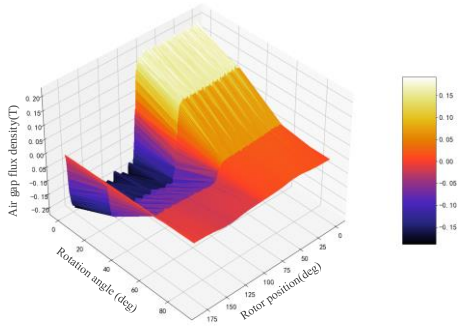

Figure 14: Air gap flux density

The main magnetic circuit of the motor is composed of air gap, stator and rotor cores, etc. The air gap flux is generated by the permanent magnet inside the rotor. Figure 14 shows the air gap magnetic density at different rotation angles of the magnetic pole. Through comparative analysis, it can be concluded that when θ=0 °, i.e. the initial angle state, the peak value of the air gap magnetic density can reach 0.22T, and the waveform has a high degree of sinusoidal, and with the increase of θ, the air gap magnetic density gradually decreases, and the weak magnetic effect is obvious.

4.5. Torque

Torque calculation formula:

$$T = p\left\{\psi_f i_q + \left(L_d - L_q\right) i_d i_q\right\}$$

Where, p is the number of poles of the motor.
Motor torque ripple definition formula:

$$T_R = \frac{T_{\max} - T_{\min}}{T_{avg}}$$

Where, T_R, $T_{\max}$, $T_{\min}$, T_{avg} They represent torque ripple, maximum torque, minimum torque and average torque respectively.

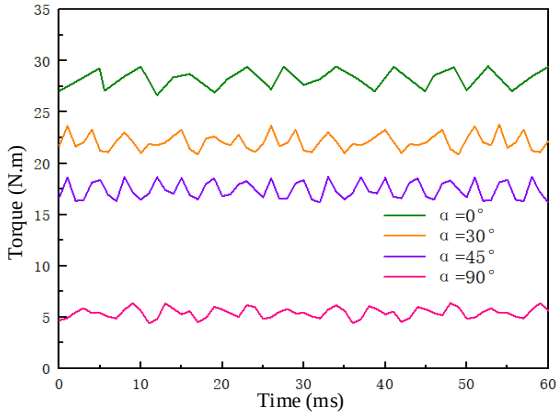

Figure 15: Torque

Table 2: Torque pulsation

α(°)	Torque Max(N•m)	Torque Min(N•m)	Average torque(N•m)	Torque ripple(%)
0	29.3	26.3	27.8	10.6
30	23.8	21.3	22.5	11.1
45	18.7	16.5	17.6	12.4
90	5.3	4.6	4.9	13.5

Figure 15 shows the relationship between torque and torque ripple at different rotation angles of the motor at rated speed. The output torque of the motor decreases with the increase of rotation Angle of permanent magnet. When θ=0°, the maximum output torque is 29N/m, When θ=90°, the minimum output torque is 5.3N/m. Table 2 shows the motor torque pulsation data under different rotation angles. It can be seen from the table that when the rotation angles of permanent magnets are 0 degrees, 30 degrees, 45 degrees and 60 degrees, the torque pulsation increases with the increase of the rotation Angle of permanent magnets. The maximum torque pulsation of the new automatic adjustable permanent magnet motor is 10.6%, 11.1%, 12.4% and 13.5%, respectively. The torque ripple value is small at 0 degrees, 30 degrees and 45 degrees. Due to the increase of air gap magnetic density harmonics and slot torque, the torque ripple is the largest at 90 degrees, which shows the rationality of the motor design.

5. Experiment

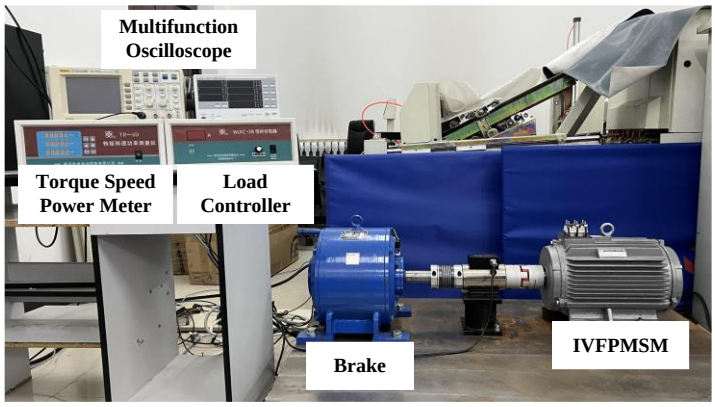

Figure 16: Prototype test platform

In order to verify the feasibility and rationality of the theoretical and simulation analysis, a prototype was made and an experimental platform was built for testing, the experimental platform is shown in Figure 16.

In order to verify the rationality of the design and the motor tuning performance, the no-load counter potential under different angles of PMs rotation was tested by motor-dragged composite drive auto-variable structure motor, respectively, and the test and simulation value were both in good sine, and the comparison graph is shown in Figure 17.

At the same time, the no-load EMF was measured. Table 3 shows the error results between the experimental and simulation values of no-load EMF. It can be seen from Table 3 that the experimental values are slightly lower than the simulation values and the error values are within 5%. The experimental results are basically consistent with the simulation results, which proves the rationality of the motor design.

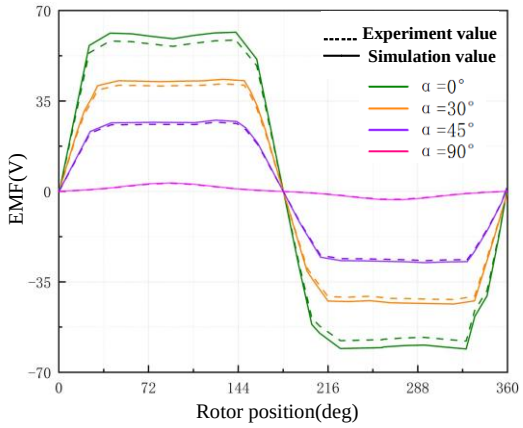

Figure 17: EMF comparison

Table 3: The experimental and simulation values

θ	Experimental/V	Simulation/V	Errors/%
0	58.5	61.6	3.1
30	42.1	43.3	1.2
45	25.2	26.7	1.5
90	3.1	3.2	0.1

6. Conclusions

In this paper, we have designed the structure of IVFPMSM and the rotor built-in drive control circuit, analyzed its operation principle and electromagnetic characteristics, built a prototype for testing, and come to the following conclusions:

The built-in automatic magnetic adjustment drive of the motor rotor has a wide range of angle adjustment, and high control accuracy, through the design of reasonable parameters, the rotor pole can be rotated 360 °, changing the traditional motor cannot achieve a wide range of permanent magnetic field adjustment and pole log adjustment.

The weakening effect of the motor is obvious, when the PMs rotation angle at 90 °, the weakening effect is about 97.5%. Through the automatic rotation of PMs, the motor can meet the needs under different complex working conditions. The reasonableness and feasibility of the motor design are verified by simulation and experiment, which has a broad application prospect.

References

[1] Song, T. F.; Liu, H. J.; Zhang, Z. Y. Topology optimization and experimental research of the interior permanent magnet synchronous motor EVs. Electric Machines and Control 2019, 23, 44-53.

[2] Zhang, L.; Zhu, X. Y.; Zuo, Y. F. Overview of fault-tolerant technologies of rotor permanent magnet brushless machine and its control system for electric vehicles. Proceedings of the CSEE 2019, 39, 1792-1802.

[3] Zhu, G. Y.; Wang, Z. J.; Zou, Y. J. Topology optimization and experimental research of the interior permanent magnet synchronous motor EVs. Electric Machines and Control 2018, 46, 111-117.

[4] Wang, F. X. Application and development tendency of PM machine in wind power generation system. Transations of China Electrotechnical Society 2012, 27, 12-14.

[5] Kou, B. Q.; Zhao, X. K. Review and analysis of electromagnetic structure and magnetic field regulation technology of the permanent magnet synchronous motor . Proceedings of the CSEE 2021, 41, 7126-7138.

[6] Zheng, P.; Wang, M. Q. Development of variable-flux machine system and its key technologies. Journal of Harbin Institute of Technology 2020, 52, 207-217.

[7] LIMSUWAN, N.; KATO, T.; KAN, A. Design and evaluation of a variable-flux flux-intensifying interior permanent-magnet machine. IEEE Transactions on Industry Applications 2014, 50, 1015.

[8] AYDIN, M.; Huang, S.; LIPO, T. A. A new axial flux surface mounted permanent magnet machine capable of field control. 37th IAS Annual Meeting, Pittsburgh, The United States, 2002.
[9] SAKAI, K.; YUKI, K.; HASHIBA, Y. Principle of the variable-magnetic-force memory motor. International Conference on Electrical Machines and Systems, Tokyo, Japan, 2010.
[10] Sun, A.; Li, j.; Qu, R. Magnetization and performance analysis of a variable-flux flux-intensifying interior permanent magnet machine. Electric Machines & Drives Conference, Coeur d'Alene, The United States, 2016.
[11] Zhou, Y.; Chen, Y.; Shen, J. X. Analysis and improvement of a hybrid permanent-magnet memory motor. IEEE Transactions on Energy Conversion 2016, 31, 915.
[12] Li, W.; CHAU, K, T.; Gong, Y. A new flux-mnemonic dual-magnet brushless machine. IEEE Transactions on Magnetics 2011, 47, 4223.
[13] Li, W.; Lee, C. H. T.; Liu, C. A dual-memory permanent magnet brushless machine for automotive integrated starter-generator application. IECON 2012—38th Annual Conference on IEEE Industrial Electronics Society, Montreal, Canada, 2012.
[14] Yang, H.; Liu, S.; Lin, N. A novel hybrid-magnetic-circuit variable flux memory machine. IEEE Transactions on Industrial Electronics 2019, 67, 52-58.
[15] Yang, H.; Zhang, H.; Lin, N. A novel variable flux dual-layer hybrid magnet memory machine with bypass airspace barriers. 2019 IEEE International Electric Machines & Drives Conference (IEMDC), San Diego, Chile, 2019.
[16] Zhang, S.; Zheng, P.; JAHNS, T. M. A novel variable-flux permanent-magnet synchronous machine with quasi-series magnet configuration and passive flux barrier. IEEE Transactions on Magnetics 2018, 54, 1.
[17] Kou, B. Q.; Li, C.; Cheng, S. A new flux weakening method of permanent magnet synchronous machine. International Conference on Electrical Machines and Systems, Nanjing, China, 2005.
[18] Zhou, G.; MIYAZAKI. T.; KAWAMATA. S. Development of variable magnetic flux motor suitable for electric vehicle. The 2010 International Power Electronics Conference-ECCE ASIA, Sapporo, Japan, 2010.
[19] Liu, X. P.; Xiao, J. J. Analysis of flux weakening performance of a novel variable flux permanent magnet synchronous machine with rotating magnetic pole. Transations of China Electrotechnical Society 2020, 35, 3182.
[20] Liu, X. P.; Zhang, Z. X.; Liu, Y. F.; Cai, S. W. Design and study of a mechanical flux-varying PM machine with auto-rotary PMs. Progress In Electromagnetics Research C 2018, 85, 221-233.